

Using a New Sky Brightness Monitor to Observe the Annular Solar Eclipse on 15 January 2010

Y. Liu · Y.-D. Shen · X.-F. Zhang · N.-P. Liu

© Springer ●●●●

Abstract For the future development of Chinese Giant Solar Telescope (CGST) in Western China, a new sky brightness monitor (SBM) has been produced for the site survey for CGST. To critically examine the performance and sensitivity of SBM, we used it in the observation of the annular solar eclipse in Dali City, Yunnan, on 15 January 2010. The observation met good weather condition with almost clear sky during the eclipse. The SBM measurement translates into the solar illuminance changes at a level of $2.4 \times 10^{-4} I_{\odot} \text{ s}^{-1}$ during the eclipse. The time of the minimal sky brightness in the field of view (FOV) is found consistent with the time of maximum eclipse. Two local sky regions in the FOV are chosen to make time series of calibrated skylight profiles. The evolution of the sky brightness thus calibrated also shows good consistency with the eclipse, particularly between the second and the third contacts. The minimal sky brightness in each local sky region took place within half a minute from the corresponding predicted contact time. Such small time delays were mainly caused by occasional cirri. The minimal sky brightness measured during the eclipse is a few millionths of I_{\odot} with standard deviation of 0.11 millionths of I_{\odot} . The observation supports that the single-scattering process (optically thin conditions) is the main contributor to the atmospheric scattering. We have demonstrated that many important aerosol optical parameters can be deduced from our data. We conclude that the new SBM is a sensitive sky photometer that can be used for our CGST and coronagraph site surveys.

Keywords: Atmospheric extinction; Earth's atmosphere; Instrumental Effects

1. Introduction

The sky brightness is a critical parameter for judging a potential site for direct coronal observation. At an excellent coronagraph site, its normalized sky brightness at noon time is usually around ten millionths of the solar disk center intensity so that it is possible for coronal emission to be reliably detected (Lin and Penn, 2004; Penn *et al.*, 2004). A couple of years ago scientists in Chinese solar physics society had reached a common understanding that they would find an excellent solar observation site in Western China before developing their next-generation large-aperture solar telescope, the Chinese Giant Solar Telescope (CGST; Fang, 2011). Based on the experience of the Advanced

National Astronomical Observatories / Yunnan Astronomical Observatory, CAS, Kunming 650011, China email: lyu@ynao.ac.cn

Table 1. Comparison of instrumental scattered light level (normalized in millionth of Sun’s disk center intensity).

Instrument	Blue	Green	Red	Water vapor
ATST SBM ¹	1.5	1.8	3.8	3.5
CGST SBM	0.77	0.81	2.12	3.26

¹Lin and Penn, 2004

Technology Solar Telescope (ATST; Keil *et al.*, 2000) site survey, they decided to adopt a sky brightness monitor (SBM) as one of the necessary tools to precisely measure the Sun’s nearby sky brightness and to provide with information on the precipitable water vapor content in the atmosphere. It should be noted that before the SBM was designed by the ATST site survey team, the traditional visual Evans sky photometer had been used for a long time since 1940’s (Evans, 1948; Lin and Penn, 2004). The SBM is actually a coronagraph instrument that is able to supply quasi-instantaneous, multi-wavelength, two-dimensional data with an automatic tracking system and a CCD system, much more objective, flexible, and powerful than the Evans sky photometer.

In January 2010 the first CGST SBM was finished in Yunnan and Nanjing optical labs. It was designed independently but has the same function as ATST SBMs (Lin and Penn, 2004), and it was equipped with a 16-bit CCD camera (SBIG402ME, 765×510 pixels). Since then, this new SBM has been used for sky brightness measurements at many different high-altitude sites of at least 3000m above sea level (Liu *et al.*, 2011a, 2011b). Important calibration parameters have also been obtained for it. The instrumental scattered light for different wavelengths are obtained to be 0.77, 0.81, 2.12, and 3.26 millionths for the blue, green, red and water vapor bandpasses, respectively. A comparison between the CGST SBM and the one used in the ATST site survey in Lin and Penn (2004) can be found in Table 1, which shows that their instrumental scattered light levels are comparable but that of the CGST SBM seems slightly better.

During the 15 January 2010 annular eclipse, we used our SBM to measure fast time variations in sky brightness in order to learn about not only the eclipse itself but also the sensitivity of SBM which had not been studied or reported before. We will introduce the observation and data analysis in Sections 2 and 3 and present the conclusions in Section 4.

2. Observation

The observation site (26°07′27″N, 099°57′15″E) of the annular eclipse was located near the Cibi lake in Dali City, Yunnan, at an altitude of 2060 m above sea level. The day was clear, sunny, and the wind was weak. The eclipse observation was made in the green wavelength band and with a highest time cadence up to 1 s. The dark-field and flat-field data had been taken for the first step correction. A sample image taken with the SBM is shown in Figure 1. The west direction is to the right, and north to the top. Two arc-shaped sky regions highlighted around the Sun were the region where local sky brightness was measured. The inner and outer radii of the two arc-regions are [4.8, 6.1] R_{\odot} from the solar center, respectively. There are totally 24378 CCD pixels in region I,

Table 2. Time table of the observations.

No.	Time	Description
1	15:07:37	First contact; start of the eclipse
2	16:40:36	Second contact
3	16:40:46	Min. brightness in sky region I
4	16:44:42	Min. brightness in full sky
5	16:44:42	Max. eclipse
6	16:48:24	Min. brightness in sky region II
7	16:48:48	Third contact
8	18:06:16	Fourth contact; end of the eclipse

and 24369 pixels in region II. It should be noted that the eclipse ended just when the sunset occurred on the top of the mountains to the west of the observing site. Therefore, some shadows of a steel tower and the mountains entered the field of view (FOV) during the late period of the eclipse. In this case, the pixels in the shadow of the tower will be deleted from our calculation. From the first contact to the third contact, the solar zenith angle was between 50° and 70° (Figure 2), and the eclipse was observed without any obscuring building or tree in this period.

The eclipse started at 15:07:37 (local standard time; hereinafter the same) when the Moon was observed transiting into the Sun's disk from its southwest limb. The eclipse ended at 18:06:16 and lasted for almost 3 h. Table 2 lists the key times for this annular eclipse. According to NASA's report (<http://eclipse.gsfc.nasa.gov/SEcat5/SE2001-2100.html>), the magnitude of this annular eclipse was 0.919, and it was the longest annular solar eclipse in this century.

3. Data Analysis

3.1. Calibration of Sky Brightness

Usually, the direct sky brightness measurements should be calibrated by normalizing each sky data with respect to the solar disk center intensity. However, it is not so straightforward in the case of an eclipse in which the solar disk center is sometimes partially and sometime totally covered by the Moon.

In our observation, in order to make a high-precision sky intensity measurement, the exposure time was preset so that the sky brightness value could fill approximately two-thirds of the full-well capacity (corresponding to 65535) of the 16-bit CCD. In this way the Sun's disk pixels, including both limb and center areas, had to become overexposed for most of the observing time. Only after 16:26 when the solar zenith angle reached 60° the readout of the limb pixels (at 0.9 radii from the disk center) dropped to below 60000.

Figure 3(a) shows raw measurements of the solar disk intensity for most of the time of this annular eclipse, with the solar disk either saturated due to CCD overexposure (before $\sim 16:05$) or occulted by the Moon ($\approx 16:05-17:30$). Figure 3(b) shows the variations in the sky illuminance (directly from the CCD readout) averaged in the sky region $[4.8, 6.1] R_{\odot}$. There is an obvious flux drop during the eclipse time. Moreover, the two flux profiles in Figure 3(c) show the variations in the sky illuminance averaged over the local regions I and II, respectively. Their profiles are similar to that of the whole sky area in Figure 3(b). Unfortunately, such sky brightness data shown in Figure 3(b) and 3(c) are not useful since no corrections for the atmospheric extinction have been made. That is, the time evolution of the sky brightness must be calibrated for further quantitative study.

When checking the data after 17:40 (Figure 3(a)), we found that the central part of the solar disk was not only exposed well but also already outside of the lunar shadow. Thus, the normalized sky brightness data between 17:40 and 18:07 (which was before the end of the observation) can supply us the opportunity to deduce the atmosphere thickness which is critical for the next calculations of solar disk center intensity for the other times.

Our calculation of air mass is based on a uniform curved atmospheric model as a function of zenith angle (Lin and Penn, 2004). Figure 3(d) presents the time evolution of our air mass model. From the theory of atmospheric extinction, the logarithm of the solar disk center intensity should be proportional to the air mass for constant extinction in cloud-free conditions (Penn *et al.*, 2004). We plot the profile of $\ln(I_{\odot})$ as a function of air mass in Figure 3(e), finding a nearly linear relation in the period between 17:40:00 and 17:58:00. This period is also shown between the vertical dashed lines in Figure 3(d). The corresponding range in the air mass $[5.19, 7.86]$ is shown between the two vertical dashed lines in Figure 3(e). With the linear relationship between $\ln(I_{\odot})$ and air mass for cloud-free conditions, the theoretical solar disk center data for the other times before 17:40:00 can be easily obtained by the extrapolation from the data between 17:40:00 and 17:58:00. The results of the fitting and extrapolation for $\ln(I_{\odot})$ as a function of air mass are shown by the dashed line in Figure 3(e). The extinction coefficient derived from the slope of the fitted line is 0.304.

Finally, by normalizing to the extrapolated solar disk center intensity and after removing the instrumental scattered light (Table 1), the time series of calibrated sky brightness have been obtained (Figure 3(f)). After the third contact the sky brightness kept increasing obviously, but at about 17:55 the CCD data in region I started to decrease significantly due to the shadow of the west mountains in this sky region. Under this condition we use the pixels in another clear sky region. At about 18:07:03 we stopped the observation when it was only a few seconds before the total sunset. Therefore, at the fourth contact at 18:06:16 when the Sun was not obscured any more by the Moon, the sky was already dark.

It should be noted that the sky brightness measurements started at 13:05, about 2 h before the first contact, but with a random time cadence and relatively scarce data samples. From the limited samples before the eclipse, we can still see that the average sky brightness kept at a stable level of about 27-34 millionths of I_{\odot} , indicating good atmospheric condition on the eclipse day which was suitable for testing a photometer.

3.2. Study of Sky Brightness

Figure 4 shows the calibrated profiles of the sky brightness before the eclipse for the two local regions I and II, respectively. Small-amplitude and slow variations can be noticed, which should reflect normal air turbulence due to, *e.g.*, occasional cirri. It can be found that before the eclipse, the difference in sky brightness between regions I and II was always within 5 millionths of I_{\odot} , but region I showed higher values for most of the time. The main reason, we suppose, should be an uneven distribution of the scattered light in SBM. For the purpose of greatly reducing the instrumental scattered light, a set of O-rings have been used and stacked along the cylindrical container of neutral density filters (ND4; 10^{-4} transmission) in front of the SBM tube. We find from the original data series (*e.g.*, Figure 1) that some stronger scattered light existed at the immediate west edges of the O-rings, just close to region I. Usually, such an uneven scattered light distribution is unnoticeable in the flat-field data. In any case, the intensity of scattered light is proportional to the incident light, and the difference in the scattered light levels in the two regions is small, so that it should not affect our examination of the sensitivity of the instrumental response to sky illuminance changes during the eclipse.

Figure 5 presents the calibrated sky brightness during the eclipse for regions I and II, and the combination of I plus II, respectively. The sky brightness in regions I and II became nearly the same before the second contact of the eclipse. For the sky region of I plus II, shown with a thin solid line for one hour including the maximum eclipse time, the sky brightness showed a profile almost symmetric in time during this period. The minimum values of the three profiles in Figure 5 are all found to occur in the period from the second to the third contact. In Table 2, we list the key times for the annular eclipse and the brightness measurements in different sky regions. From this comparison, good time correspondence is found between the contacts and their accompanying sky brightness changes. Within the measurement accuracy, we find no time difference among the maximum eclipse and the minimum brightness in the FOV. This good temporal coincidence indicates that our SBM is a sensitive photometer that can track rapid changes in the sky brightness during the eclipse.

Moreover, in region I the sky brightness dropped to the minimum 10 s after the time of the second contact, while in region II it occurred 24 s before the time of the third contact. These small time differences between the observed minima in sky brightness and the theoretical expectations may indicate some weak atmospheric turbulence due to dust, cloud, or other components that are not easily noticed by eye but can be detected by the SBM instrument. There was a 7.5 min difference between the sky brightness minima in regions I and II. This time difference, almost equal to the time between the second and the third contact, suggests that the atmospheric scattering process in each sky region should be independent from each other in some degree, which we will try to study in the next section.

3.3. Comparison with Simulation and Theory

For comparison, we have carried out a simulation of the annular eclipse and calculated its normalized illuminance above the terrestrial atmosphere (Figure 6(a-b)), based on the eclipse magnitude and the limb darkening parameters (Livingston, 2000). An animation movie from the simulation is available in the online journal. The normalized

illuminance profile is shown in Figure 6(b), with the minimum value of 0.108. Figure 6(c) shows a photograph of the annular eclipse taken at the maximum obscuration. In Figures 3(f), 5, and 6, a flat-bottom feature of about 8 min width can be noticed in the valley part of the profiles around the eclipse maximum. A close-up plot including this feature is shown in Figure 7 over a shorter period including the second and the third contacts.

The profile of the normalized solar illuminance obtained in the simulation, multiplied by a factor of 70, is also shown as the dashed line in Figure 7. The thin solid line represents the profile of the combination area of I plus II after shifting down by 4.46, *i.e.*, $B_I + B_{II} - 4.46$. It can be clearly seen that the two profiles fit well with each other during the period from the second contact to the third contact. The standard deviation between the two profiles over this period is only 0.11 millionths of I_\odot , suggesting high sensitivity of our SBM instrument to weak signals.

The two arrows in Figure 7 denote the minima in the profiles for regions I and II, respectively. The minimum of region I was obviously earlier than that of region II. In the eclipse observation, the Moon started to transit from the southwest side of the solar disk. That is, the place for the first two contacts to occur was closer to region I than to region II, indicating that the single-scattering process (optically thin conditions) should be the main contributor to the atmospheric scattering.

In the following, the classical theory on sky radiation under the condition of single scattering is used to deduce the sky brightness in a homogeneous atmosphere (González Jorge *et al.*, 1998; Lin and Penn, 2004; Huang, 2008). According to those theories the normalized sky brightness at a wavelength λ along the line of sight (LOS) is:

$$\begin{aligned} B_\lambda(\hat{\mathbf{n}}) &= \frac{I_\lambda(\hat{\mathbf{n}})}{I_\lambda(\hat{\mathbf{n}}_\odot)} \\ &= \Phi_\lambda(\hat{\mathbf{n}}) \cdot \kappa_\lambda \cdot M(\hat{\mathbf{n}}) + B'_\lambda \\ &\simeq \Phi_\lambda(\hat{\mathbf{n}}) \cdot \kappa_\lambda \cdot M(Z_\odot) + B'_\lambda, \end{aligned} \quad (1)$$

where $\hat{\mathbf{n}}$ is the unit vector along LOS, $\hat{\mathbf{n}}_\odot$ the unit vector from the observer to the solar disk center, and κ_λ the extinction coefficient. $M(Z_\odot)$ is the air mass along the direction of the Sun, and Z_\odot is the zenith angle, *i.e.*, the zenith distance of the Sun. In our observation, since the sky regions were close to the Sun, it can be considered that $M(\hat{\mathbf{n}}) \simeq M(Z_\odot)$. B'_λ is an instrumental constant which depends on the wavelength. Φ is the angular (scattering) phase function, describing the fall of the sky brightness distribution when moving away from the solar limb, which can be expressed as follows:

$$\Phi_\lambda(\hat{\mathbf{n}}) = \frac{1}{4\pi} \int_{\Delta\omega_{\hat{\mathbf{n}}_\odot}} P(\hat{\mathbf{n}}, \hat{\mathbf{n}}') \frac{I_\lambda^0(\hat{\mathbf{n}}')}{I_\lambda^0(\hat{\mathbf{n}}_\odot)} d\omega_{\hat{\mathbf{n}}'}, \quad (2)$$

where $\Delta\omega_{\hat{\mathbf{n}}_\odot}$ is the solid angle subtended by the solar disk as viewed from the observer in the terrestrial atmosphere. $I_\lambda^0(\hat{\mathbf{n}})$ is the solar illumination function outside the terrestrial atmosphere, and it actually provides the center-to-limb variation. In the visible wavelength range it is the well-known limb darkening function. P , the so-called adequate phase function (Chandrasekhar, 1950; Pillet *et al.*, 1990) describing the scattering pro-

cess, can be practically given by the Henyey-Greenstein phase function (Henyey and Greenstein, 1941):

$$P = \frac{1 - g^2}{[1 + g^2 - 2g \cos \theta]^{3/2}}, \quad (3)$$

in which,

$$\cos \theta = \hat{\mathbf{n}} \cdot \hat{\mathbf{n}}', \quad (4)$$

and the free parameter (g) gives the angular dependence of the scattered light with $g = 1, 0, -1$ for forward, isotropic, and backward scattering, respectively. From our simulation based on Equation (3), P is found sensitive to the scattering angle factor $\cos \theta$ for a given value of g .

On the other hand, for a given direction $\hat{\mathbf{n}}$, g (thus, the angular phase function Φ) and M can be thought constant during a short time (*e.g.*, from the second contact to the third). The evolution of the sky brightness in this direction shall be dependent on the solar radiation function in the same direction. During an eclipse the Moon just plays the role to ‘cut’ the direct solar radiation from the space, resulting in a zero solar radiation function which will significantly reduce the sky brightness in its shadow, accordingly. Therefore, it is not difficult to understand there is a time difference (7.5 min) for the minima in regions I and II. Moreover, the non-zero sky brightness for the minimum in each sky region should be mainly contributed by the atmospheric scattering from the other part of the solar disk that was not occulted by the Moon. We expect a near zero sky brightness minimum for a total solar eclipse.

4. Discussion and Conclusions

For the purpose of CGST and coronagraph site survey in Western China, we had recently developed a new SBM following the ATST team’s experience. During the Dali annular eclipse on 15 January 2010, we used it to measure the sky brightness to test its performance and sensitivity. The sky was clear and sunny on that day, and the eclipse ended just before the time of the local sunset.

The calibration of the sky brightness data is special for the case of the eclipse. In order to obtain the theoretical solar disk center intensity, we used the extrapolation method (Penn *et al.*, 2004) and the uniform curved atmospheric model (Lin and Penn, 2004) based on the data available between 17:40 and 18:07. Because of the nice atmospheric condition during the observation, the air mass and the theoretical solar intensity data were successfully obtained from the short-term observation.

We have calculated the sky brightness for the FOV and two local sky regions around the solar disk (Figure1). These sky brightness profiles show a common, flat-valley feature between the second and the third contacts. The noise signal due to local atmospheric turbulence was clearly seen through the comparison between the observation and the simulation (see the upper two lines in Figure 7). It is interesting to find that the times of their minimum showed good agreement with the eclipse stages. The brightness minimum of the whole FOV occurred just at the same time of the maximum eclipse (Table 2). The minimum in the sky brightness took place 10 s later (24 s earlier) than the second (third) contact for region I (II) which is at the west (east) side of the solar

disk, respectively. These two time differences, although small, suggest us that it is better to calculate the sky brightness using the sky area as large as possible in the FOV for the site survey work. As a matter of fact we found no time delay for the whole FOV data.

On the other hand, we have noticed a 7.5 min time difference between the sky brightness minima in regions I and II. The time difference actually corresponds to the period from the second to the third contact of the eclipse. This phenomenon supports that single scattering is the main scattering process in the terrestrial atmosphere, and multiple scattering can be ignored for optically thin conditions.

Moreover, we have noticed that the lowest sky brightness values obtained by the SBM were only a few millionths of I_{\odot} for this eclipse between the second and the third contacts (Figure 7). We can use these measured low sky brightness, together with other parameters from the calculations and simulations as mentioned above, to further investigate the scattering process in the atmosphere. One of the advantages of the 15 January 2010 solar annular eclipse, is that it offered us the longest time for a high-precision measurement of the sky brightness from the second contact to the third one. Here, based on some reasonable assumptions, we will deduce and estimate the free parameter g in the Henyey-Greenstein phase function in Equation (3). The angular dependence of the scattered light is determined by g ; therefore it is an important parameter for diagnosing optical properties of aerosol.

Since the observed regions I and II were close to the Sun, we can simplify the Henyey-Greenstein phase function to be:

$$P = \frac{1 + g}{(1 - g)^2}, \quad (5)$$

with $\cos \theta \simeq 1$. On the other hand, based on Equations (1) and (2), P can be expressed by:

$$P = \frac{4\pi BL^2}{(1 - m^2)\kappa_{\lambda} M I_{\lambda}^1}, \quad (6)$$

in which all the physical and geometrical parameters are nondimensional numbers. That is, B is the calibrated sky brightness, L is the Sun-Earth distance in unit of solar radius, m is the magnitude of the annular eclipse, κ_{λ} is the extinction coefficient, M is the air mass, and I_{λ}^1 is the normalized solar illuminance. Because the parameters on the right-hand side of Equation (6) have been known from the last sections for the time of the maximum eclipse (16:44:42), g can be solved out from Equations (5) and (6). The result and the parameters involved in the calculation are listed in Table 3. The value of g , 0.912, indicates a strong forward-scattering feature in the atmosphere for Dali city, Yunnan.

If we adopt a simple model of plane-parallel atmosphere, our SBM measurement can be translated into the changes in solar illuminance as small as $2.4 \times 10^{-4} I \text{ s}^{-1}$ (from Figure 6) during the eclipse, where I is the Sun's illuminance without any obscuration by the Moon. For comparison, a large impulsive X-ray flare can contribute to the solar illuminance increase in the whole visible spectral region like $1.1 \times 10^{-4} I \text{ s}^{-1}$ (Švestka, 1976). Thus we are satisfied with the SBM sensitivity.

In 2011 US National Solar Observatory had shipped their SBM system to us for calibrating the CGST SBM. The calibration data have been obtained and further calibration results will be shown in another paper.

Table 3. Nondimensional parameters for atmospheric optical properties derived at the maximum eclipse. See the text for definitions

Time	B	L	m	κ_λ	M	I_λ^1	g
16:44:42	6.22×10^{-6}	215.1	0.919	0.304	2.53	0.108	0.912

There will be another annular eclipse to occur soon on 21 May 2012 in southeast of China. The difference is that this eclipse will happen near sunrise. We need to preset proper exposure times for the SBM to measure the brightness of the sky and the photosphere simultaneously in all four wavelengths, in order to reveal more information about the scattering process in the atmosphere.

Acknowledgements The authors thank the referee and the editor for many useful suggestions which improved the manuscript. This work has obtained encouragements and assistance from many colleagues. We thank especially Hai-sheng Ji, Hui Li, Bai-rong Zhang, Ming-chan Wu, Ke Lou, Zhong Liu, Jun Lin, Lei Yang, Hou-kun Ni and Haiying Zhang for discussion and support. This work is supported by the Natural Science Foundation of China (Grant Nos. 10933003, 11078004, and 11073050) and the National Key Research Science Foundation (MOST 2011CB811400).

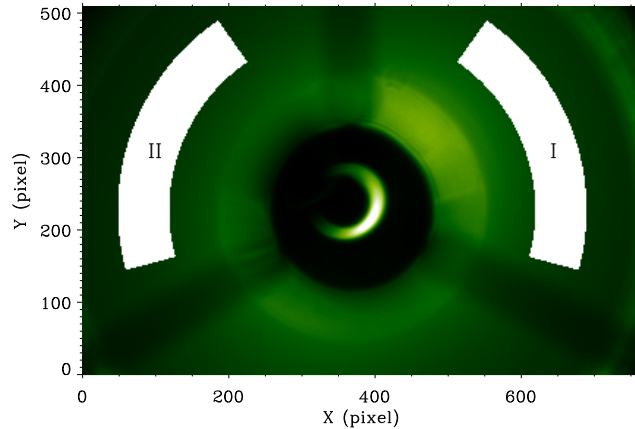


Figure 1. A sample eclipse image taken by SBM in the green band. Two arc-shaped sky regions, marked with ‘I’ and ‘II’, are the regions where we analyzed the sky brightness in detail. The central region shows the eclipsed solar disk filtered by the neutral density occulter. The shadows are due to three occulter support arms. Outside of this occulter region are bright diffraction rings from the occulter edges. Diffraction from the front of the telescope tube can be seen at the rightmost edges of the field of view.

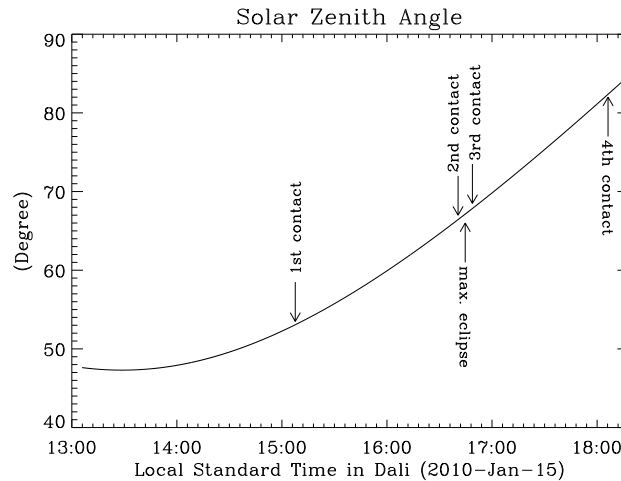


Figure 2. Evolution of the solar zenith angle during the observation. Five vertical arrows show the moments of contact and the maximum eclipse.

References

- Chandrasekhar, S.: 1950, *Radiative Transfer*, Oxford Univ. Press, London and New York, 5.
 Evans, J.-W.: 1948, *J. Opt. Soc. Am.* **38**, 1083.
 Fang, C.: 2011, *Res. Astron. Astrophys.* **11**, 1377.
 González Jorge, H., Martínez Pillet, V., Vázquez, M., Pallé, P., McGovern, F., Raes, F.: 1998, *New Astron. Rev.* **42**, 515.
 Henyey, L.-G., Greenstein, J.-L.: 1941, *Astrophys. J.* **93**, 70.
 Huang, J.: 2008, *J. Spacecraft TT&C Tech.* **27**, 61.
 Keil, S.-L., Rimmele, T.-R., Keller, C., Hill, F.: 2000, *Bull. Am. Astron. Soc.* **32**, 1433.
 Lin, H., Penn, M.-J.: 2004, *Pub. Astron. Soc. Pac.* **116**, 652.
 Liu, N., Liu, Y., Shen, Y., Zhang, X., Cao, W., Jean, A.: 2011, *Acta Astron. Sinica.* **52**, 161 (in Chinese).

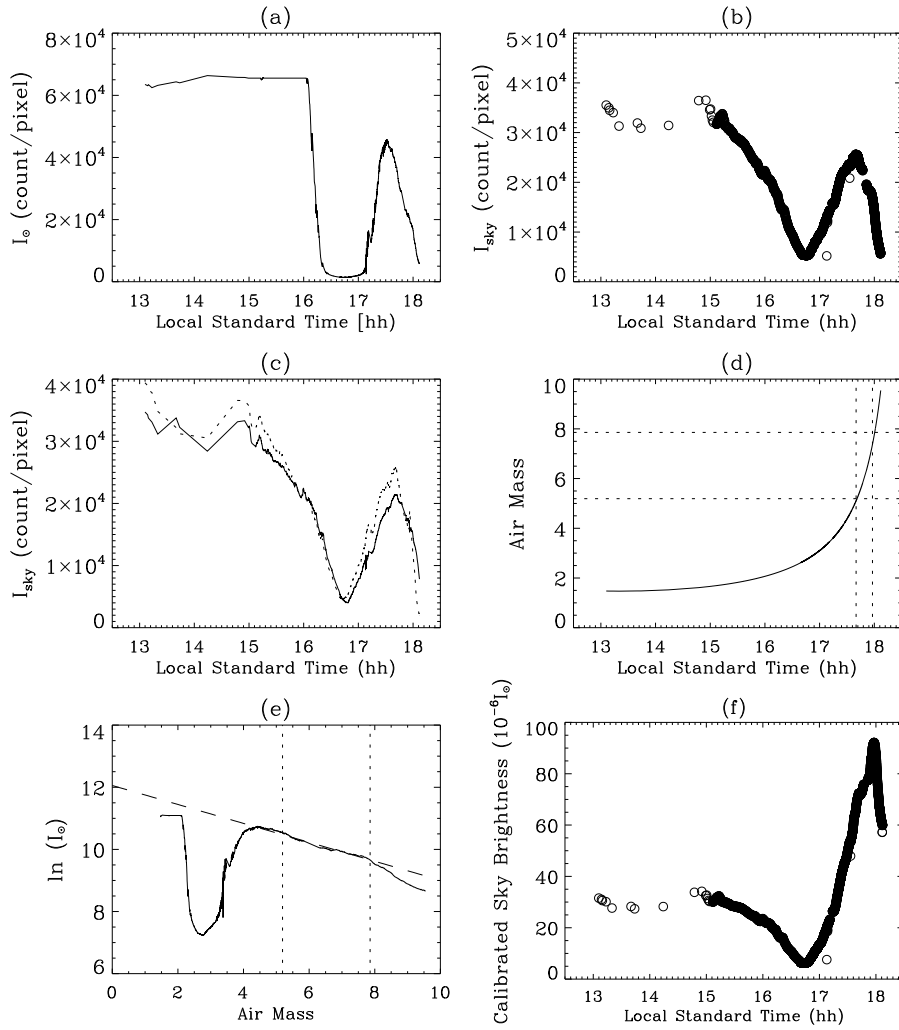


Figure 3. (a) Time profile of un-calibrated I_{\odot} . (b) Time profile of un-calibrated I_{sky} . (c) Two time profiles of calibrated I_{sky} for regions I (dashed curve) and II (solid curve), respectively. (d) Time profile of air mass. (e) Profile of $\ln(I_{\odot})$ as a function of air mass. The data between the two vertical lines are used to extrapolate $\ln(I_{\odot})$ as is shown with the inclined dashed line. (f) Time profile of the calibrated sky brightness.

- Liu, N., Liu, Y., Shen, Y., Zhang, X., Cao, W., Jean, A.: 2011, *Chin. Astron. Astrophys.* **35**, 428.
 Livingston, W.C.: 2000, In: Cox, A. N. (ed.) *Allen's Astrophysical Quantities*, Springer Verlag, London, 355.
 Martínez Pillet, V., Ruiz Cobo, B., Vázquez, M.: 1990, *Solar Phys.* **125**, 211.
 Penn, M.-J., Lin, H., Schmidt, A.-M., Gerke, J., Hill, F.: 2004, *Solar Phys.* **220**, 107.
 Penn, M.-J., Lin, H., Tomczyk, S., Elmore, D., Judge, P.: 2004, *Solar Phys.* **222**, 61.
 Švestka, Z.: 1976, *Solar Flares*, D. Reidel Publ. Co., Dordrecht, 13.

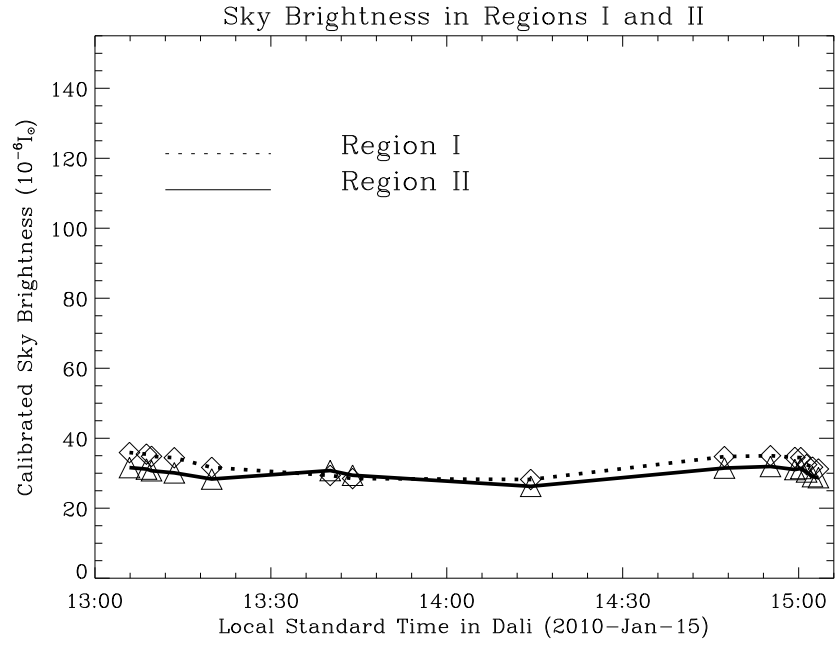


Figure 4. Time profiles of calibrated sky brightness for the two regions I (thick dotted line) and II (thick solid line) before the start of the annular eclipse.

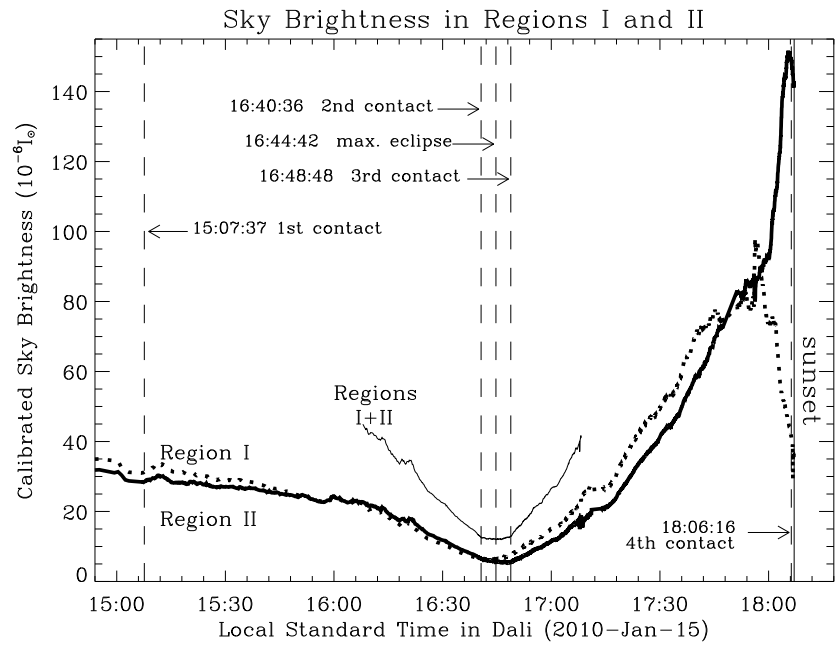


Figure 5. Time profiles of calibrated sky brightness for regions I (dotted line), II (thick solid line) and I+II (thin solid line) during the annular eclipse.

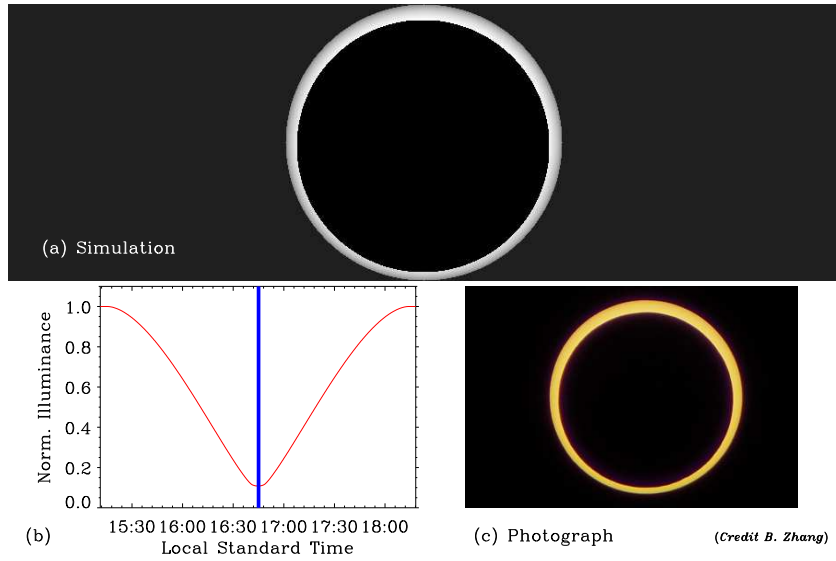


Figure 6. (a) Simulation of the annular eclipse. An animation file is available in the online journal. (b) Normalized solar illuminance during the eclipse based on the simulation. (c) A sample eclipse photograph.

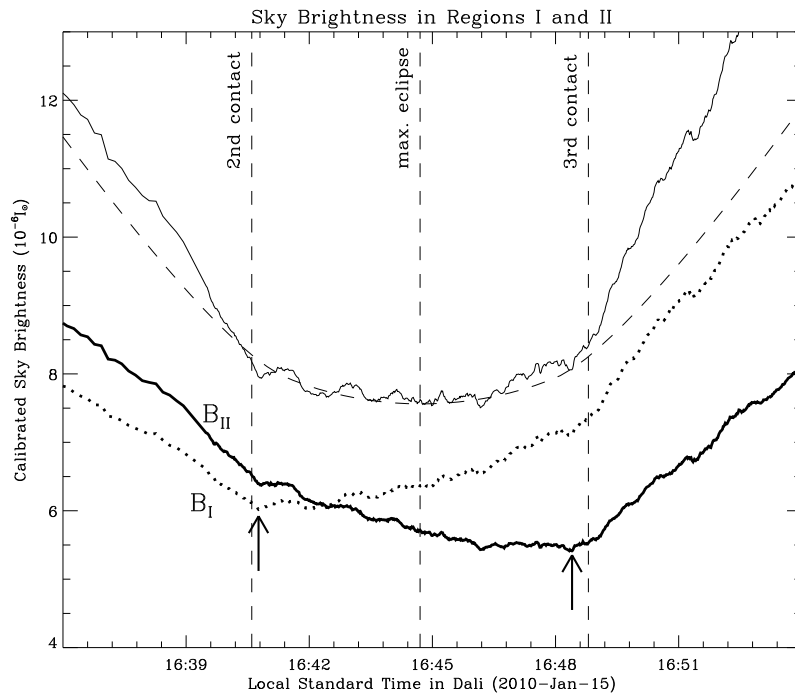


Figure 7. Time profiles of calibrated sky brightness for regions I (thick dotted line), II (thick solid line) and I+II (thin solid line, shifted down along the ordinate; see text) during the annular eclipse. The dashed line represents the normalized solar illuminance simulated in Figure 6 (multiplied by a factor; see text). The two arrows point to the minimum sky brightness in regions I and II.

